Title

αB-Crystallin overexpression in astrocytes modulates the phenotype of the BACHD mouse model of Huntington's disease

Journal

Human Molecular Genetics, 25(9)

ISSN

0964-6906

Authors

Oliveira, Ana Osório
Osmand, Alexander
Outeiro, Tiago Fleming
et al.

Publication Date

2016-05-01

DOI

10.1093/hmg/ddw028

Peer reviewed

OXFORD

Human Molecular Genetics, 2016, Vol. 25, No. 9 1677–1689

doi: 10.1093/hmg/ddw028
Advance Access Publication Date: 26 February 2016
Original Article

ORIGINAL ARTICLE

αB-Crystallin overexpression in astrocytes modulates the phenotype of the BACHD mouse model of Huntington's disease

Ana Osório Oliveira[1,2,3], Alexander Osmand[4], Tiago Fleming Outeiro[2,5,6], Paul Joseph Muchowski[7] and Steven Finkbeiner[3,8,9,10,*]

[1]Lisbon Academic Medical Center PhD Program, [2]Cell and Molecular Neuroscience Unit, Instituto de Medicina Molecular, Faculdade de Medicina de Lisboa, Universidade de Lisboa, Lisbon, Portugal, [3]Gladstone Institute for Neurological Disease, J. David Gladstone Institutes, San Francisco, CA, USA, [4]Department of Biochemistry and Cellular and Molecular Biology, University of Tennessee, Knoxville, TN, USA, [5]CEDOC—Chronic Diseases Research Center, Faculdade de Ciências Médicas, Universidade Nova de Lisboa, Lisbon, Portugal, [6]Department of Neurodegeneration and Restorative Research, University Medical Center Goettingen, Goettingen, Germany, [7]Soteria Therapeutics, San Francisco, CA, USA, [8]Department of Neurology, [9]Department of Physiology, University of California at San Francisco, San Francisco, CA, USA and [10]Taube/Koret Center for Neurodegenerative Disease Research, San Francisco, CA, USA

*To whom correspondence should be addressed at: Gladstone Institute of Neurological Disease, 1650 Owens St., San Francisco, CA 94158, USA. Tel: +1 415734 2508; Email: sfinkbeiner@gladstone.ucsf.edu

Abstract

Huntington's disease (HD) is caused by an expanded polyglutamine (polyQ) tract in the huntingtin (htt) protein. The polyQ expansion increases the propensity of htt to aggregate and accumulate, and manipulations that mitigate protein misfolding or facilitate the clearance of misfolded proteins are predicted to slow disease progression in HD models. αB-crystallin (αBc) or HspB5 is a well-characterized member of the small heat shock protein (sHsp) family that reduces mutant htt (mhtt) aggregation and toxicity *in vitro* and in *Drosophila* models of HD. Here, we determined if overexpressing αBc *in vivo* modulates aggregation and delays the onset and progression of disease in a full-length model of HD, BACHD mice. Expression of sHsps in neurodegenerative disease predominantly occurs in non-neuronal cells, and in the brain, αBc is mainly found in astrocytes and oligodendrocytes. Here, we show that directed αBc overexpression in astrocytes improves motor performance in rotarod and balance beam tests and improves cognitive function in the BACHD mice. Improvement in behavioral deficits correlated with mitigation of neuropathological features commonly observed in HD. Interestingly, astrocytic αBc overexpression was neuroprotective against neuronal cell loss in BACHD brains, suggesting αBc might be acting in a non-cell-autonomous manner. At the protein level, αBc decreased the level of soluble mhtt and decreased the size of mhtt inclusions in BACHD brain. Our results support a model in which elevating astrocytic αBc confers neuroprotection through a potential non-cell-autonomous pathway that modulates mhtt aggregation and protein levels.

Received: September 3, 2015. **Revised and Accepted:** February 1, 2016

Introduction

Huntington's disease (HD) is a fatal autosomal, dominantly inherited, progressive neurodegenerative disorder (1). The mutation responsible for HD leads to abnormally long CAG/polyglutamine (polyQ) repeats in the IT15 gene, which encodes the ubiquitously expressed protein huntingtin (htt) (2). The polyQ expansion makes htt prone to misfold and accumulate, which is thought to confer a toxic gain of function (3). The deposition of inclusion bodies of misfolded htt fragments containing the expanded polyQ region is a neuropathological hallmark of HD (4).

This accumulation of misfolded proteins in cells triggers a protective stress response that includes the up-regulation of heat shock proteins (Hsps) that function as molecular chaperones either to prevent protein misfolding or to rescue misfolded proteins to help restore cellular homeostasis (5,6). Overexpression of molecular chaperones reduces htt aggregation and increases lifespan in HD *Drosophila* and mice (7–10). Manipulating the expression of chaperones that mitigate protein misfolding or facilitate its clearance may represent an approachable therapeutic target to decrease toxicity and slow disease progression in HD models.

The small Hsp (sHsp) family of molecular chaperones includes proteins of small molecular mass (15–30 kDa) that accumulate in the cells after many different environmental, physiological or pathological stresses (11). sHsps are protective in many pathways that are implicated in HD, including native and non-native protein folding, cytoprotection from numerous stresses, such as oxidative damage and modulation of cell death, and survival pathways (6). Structurally, all sHsps share a central C-terminal domain, referred to as the alpha-crystallin domain, consisting of 80–90 residues in eight beta strands that form an intermolecular beta-sheet interaction site (12,13). The most studied sHsps (i.e. Hsp27/HspB1, αA-crystallin/HspB4, αB-crystallin/HspB5, Hsp22/HspB8 and Hsp16.2/HspB11) have strong anti-aggregation chaperone activity through their ability to recognize and interact with partially folded protein intermediates (14,15). Chaperones include eligible candidates for neuroprotection in HD (6,16), and their potential has been evaluated *in vitro* (17), in *Caenorhabditis elegans* (18), mammalian cells (8,19) and *in vivo* models of HD (20). Our study focused on the αB-crystallin (αBc) or HspB5 protein. This sHsp has a chaperone-like function and binds to the unfolded proteins to inhibit its aggregation (21), suggesting that αBc has an impact on several protein conformation disorders. αBc prevents the aggregation and elongation of α-synuclein fibrils (22,23), implicated in Parkinson's disease (PD). Furthermore, αBc is a potent inhibitor of amyloid fibril formation and, by slowing the rate of its aggregation, effectively reduces the toxicity of amyloid-β peptide in cells (24), suggesting a protective role for αBc in a Alzheimer's disease (AD) *in vitro* model. Amyotrophic lateral sclerosis (ALS) is a progressively paralytic neurodegenerative disease that can be caused by mutations in Cu,Zn-superoxide dismutase 1 (SOD1). Completely eliminating αBc in mice expressing two different SOD1 mutants (G37R and L126Z) reduced the interval to disease end stage by 20–30 days in mice expressing either mutant (25). These results suggest that the activity of αBc modulates the cellular specificity of mutant SOD1 accumulation. In addition, overexpression of αBc in a mouse model of Alexander disease (AxD), a rare and fatal neurodegenerative disorder of childhood, rescued the AxD mice from terminal seizures. Consistently, loss of αBc resulted in increased mortality of these mice (26).

We previously showed that expressing a mutant htt (mhtt) fragment in the lens of mice lacking αBc markedly accelerated the onset and severity of mhtt aggregation (27). In addition, overexpression of αBc in a transgenic drosophila model of HD suppressed mhtt toxicity, suggesting a protective role for αBc in HD (28). Downregulation of a number of molecular chaperones, including αBc, was reported in the brains of the exon-1 fragment mouse model R6/2 (20,29), suggesting αBc may be associated with HD pathogenesis *in vivo*, and that restoration of chaperone levels could be neuroprotective against disease. Interestingly, current evidence suggests expression of the sHsps, such as αBc, is predominantly in non-neuronal cells (7). In the brain, αBc is mainly found in astrocytes and oligodendrocytes. The role of astrocytes and oligodendrocytes in HD is not entirely clear. However, evidence suggests that non-cell-autonomous functions of glial cells are an important mechanism of supporting neuronal health (30). We focused on astrocytes because recent studies in different HD mice models have shown that astrocytes contribute to neuronal dysfunction *in vivo*, by a marked decreased expression of both glutamate transporters, GLAST and GLT-1, and of glutamate uptake (31), by a decrease on potassium (K+) ion channel expression in astrocytes and disturbances of astrocyte-mediated K(+) homeostasis (32) or by being a source of oxidative stress to neurons *in vivo* (33).

Here we investigated the effects of αBc overexpression in astrocytes on behavioral and neuropathological phenotypes in a full-length HD mouse model, BACHD. These mice exhibit early (2–3 months of age) robust and progressive motor deficits, and late-onset selective neuropathology, including significant cortical and striatal atrophy (34). αBc astrocytic overexpression in BACHD mice improved motor and cognitive symptoms. The improvements in behavioral deficits correlated with prevention of the cortical and striatal neuron loss that is observed in HD. We observed a decreased level of soluble mhtt, and decreased size of mhtt inclusions in BACHD brain. Our results suggest that αBc is protective in HD through an astrocyte-mediated chaperone function related to regulating mhtt protein levels and aggregation in BACHD brains.

Results

αBc levels decrease over time in BACHD mice

Sequestering chaperones into aggregates decreases the number of soluble chaperones that are available in the cell, and this presumably enhances abnormal protein folding (20). Levels of αBc and other chaperones decrease in the brains of an exon1 fragment HD model (29). Although mhtt exon1 is sufficient to cause disease, it lacks features of full-length htt, such as post-translational modification sites, and protein interaction or signaling domains that may be important for regulating htt proteostasis and toxicity. We wanted to determine if a decrease in endogenous αBc levels is altered during the progression of disease in the full-length mouse model of HD—BACHD mice. This model shows a robust phenotypic behavioral deficit and neuropathological features, and full-length mhtt expression with 97 polyQ is governed by the human Htt promoter, and so, it presumably recapitulates any cell- and time-dependent expression patterns seen in humans (35).

Whole-brain lysates from BACHD mice and wild-type (WT) littermates from 3, 6, 9 and 12 months, corresponding to early- and late-onset stages of disease, were harvested. At 3 and 6 months of age, the protein levels of αBc were not different in BACHD and WT mice. However, at 9 and 12 months of age, BACHD mice had significantly lower brain levels of αBc than WT littermates (Fig. 1). The decreased protein levels of αBc over

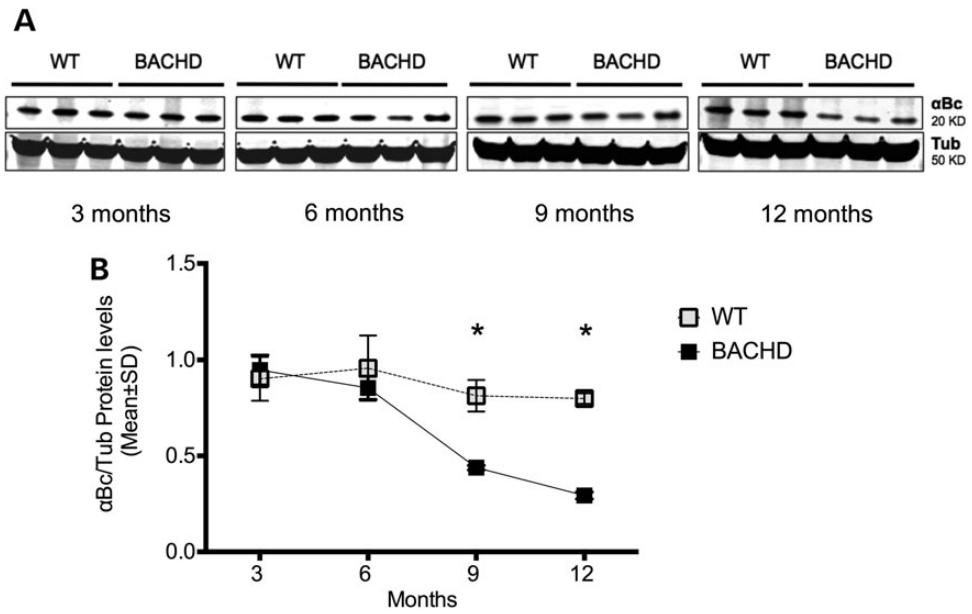

Figure 1. αBc levels decrease over time in BACHD mice. (**A**, **B**) BACHD ($n = 5$) and WT ($n = 5$) littermates were sacrificed at 3, 6, 9 and 12 months of age. Protein levels of αBc were determined by western blot analysis with whole-brain homogenates of BACHD and WT mice. (**A**) Immunoblots showing αBc protein level is decreased in BACHD, in an age-dependent manner, specifically after 6 months (when the motor symptoms are more robust in this mice model). (**B**) Respective quantifications of protein levels of αBc normalized to anti-β-tubulin (to show relative loading levels). Error bars represent standard errors of the mean (means ± SEM). Data were tested for statistically significant differences using *t*-tests (*$P < 0.05$; **$P < 0.01$).

time in BACHD mice, especially after 6 months, correspond to the period where the behavioral and motor deficits in BACHD mice begin to be clearly detected (21). These data raise the possibility that a decline in αBc protein levels is involved in mediating pathogenesis.

Overexpression of αBc in astrocytes improves motor performance in BACHD mice

To determine if the decline in αBc levels is an incidental finding or is playing a role in disease progression in BACHD mice, we sought to overexpress αBc and determine if it affected disease-associated phenotypes. To do so, we crossed BACHD mice with transgenic mice expressing the WT αBc gene, Cryab. Since aBc is predominantly expressed in glia, we chose a model in which Cryab is under the control of the human GFAP promoter that targets expression to astrocytes (26). We evaluated motor behaviors at 3, 7, 10 and 13 months of age. These ages in mice correspond to early-, mid- and late-stage disease with regard to symptomatology and neuropathology (34). Deficits in rotarod latency to fall (34,36) and balance beam latency to cross (37,38) were previously reported in BACHD. In these assays, BACHD mice had performance deficits in an age-dependent manner (Fig. 2). In our study, BACHD behavioral deficits were detected as early as 3 months of age in rotarod and balance beam tests. BACHD mice fall off an accelerating rotarod sooner than WT littermates and Cryab Tg mice (significant at 3, 7, 10 and 13 months), and this effect is partially rescued by astrocytic overexpression of the Cryab transgene in BACHD mice (double transgenic, DTg) at all time points tested (Fig. 2A).

During the balance beam evaluation, the mice cohort was tested with a large-sized and a medium-sized balance beam (39). For our analyses, we used the data from the medium beam, which requires more motor coordination to cross than the large beam. BACHD mice took significantly more time to cross the medium beam than WT and Cryab Tg mice at 3, 7, 10 and 13 months (Fig. 2B). αBc overexpression rescues this phenotype in BACHD only at the 7 months; therefore, αBc does not improve the overall latency to cross the balance beam of the BACHD mice (Fig. 2B). We also tested the ability to stay on the beam by measuring the number of slips and falls. DTg mice were significantly better on the medium beam than BACHD with fewer slips (Fig. 2C) and falls (Fig. 2D) at later stages of disease progression. The number of slips and falls of Cryab Tg mice was similar to WT mice (Fig. 2C and D). These results indicate a specific genetic interaction of αBc and mhtt that mediates the onset and severity of motor deficits in BACHD mice as measured by balance beam and rotarod assays.

We found that BACHD and DTg mice gain significantly more weight (an average of 20–30%) than WT and Cryab Tg controls, between 3 and 7 months until 13 months of age (Supplementary Material, Fig. S2). Since weight could affect motor performance, we examined the relationship of weight and rotarod and balance beam performance in BACHD mice. We found that the rotarod and balance beam performance in this cohort of BACHD and DTg mice at 3, 7, 10 and 13 months was not significantly correlated with body weight (Supplementary Material, Fig. S3). Therefore, the improvement seen in the DTg is not explained by weight differences or the effect of weight on motor performance. Thus, we conclude that astrocytic αBc positively affects BACHD motor performance.

Expression of αBc in astrocytes improves strategy shifting in BACHD mice

In addition to motor performance, BACHD mice also exhibit cognitive decline at a later stage of the disease (40,41), similar to what is observed in HD patients (42,43). Therefore, we wanted to examine the effect of αBc overexpression on cognitive performance in a sensitive striatal learning-dependent assay, the swimming T-maze test. We used this test to measure procedural and spatial learning in symptomatic BACHD at the last time point of

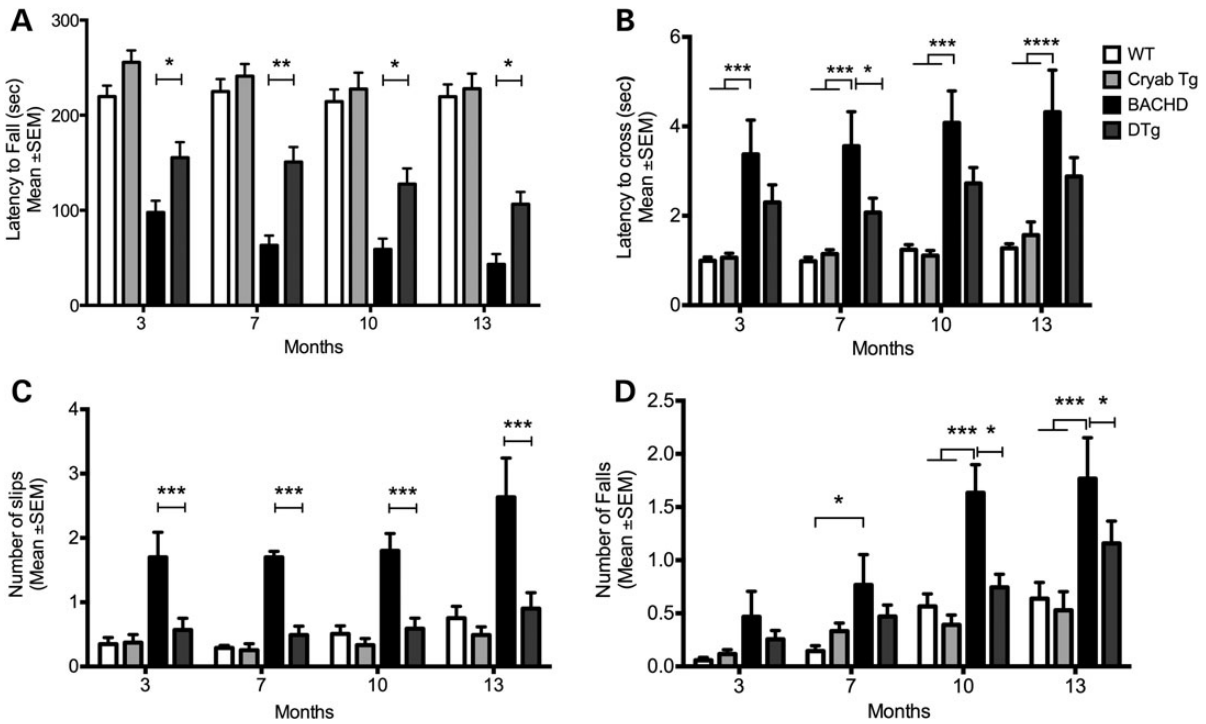

Figure 2. αBc overexpression improves behavioral readouts in BACHD mice. Behavioral readouts of disease progression in BACHD were measured at 3, 7, 10 and 13 months of age using rotarod and balance beam. Data at each time point were tested for statistically significant differences using two-way ANOVA with multiple comparisons tests corrected by Tukey post-hoc tests. At 3 months of age, group sizes were as follows: WT ($n = 20$), Cryab Tg ($n = 19$), BACHD ($n = 14$), DTg ($n = 17$). Values are means ± SEM. $^{*}P < 0.05$, $^{**}P < 0.01$ or $^{***}P < 0.001$ for main effect of the BACHD transgene by two-way ANOVA. (**A**) Rotarod. BACHD mice fall off an accelerating rotarod sooner than WT littermates and Cryab tg mice (significant main effect of the BACHD transgene). αBc overexpression partially rescues the BACHD motor impairment on DTg mice, and this is significant at all different time points at 3, 7, 10 and 13 months. (**B**) BACHD mice take significantly more time to cross the balance beam than WT littermates and Cryab tg mice. (**C, D**) The BACHD group also showed significant higher number of slips and falls during this task. αBc overexpression reduces the number of slips (**C**) and falls (**D**) in BACHD mice during the balance beam test. αBc overexpression does only change the overall latency to cross in DTg mice at 7 months, however, reduces significantly the number of slips (7, 10 and 13 months) and falls (10 and 13 months) of BACHD mice in the balance beam transversal assay.

behavioral evaluation, when the mice were 13 months of age (a time known for more accentuated neurobehavioral dysfunction and cognitive decline in BACHD mice). The test was performed at only one time point in the course of disease progression to avoid any bias related to recall or long-term memory of the task. This task was previously tested in a different mouse model of full-length htt, YAC128 mice, as a simple two-choice test of striatal dependent-learning and memory to facilitate rapid training and testing in visually cognitive-impaired mice (44). A schematic representation of the water T-maze task is presented in Figure 3A. Briefly, on the first day, the mice were trained to swim and enter the correct arm on the T-maze, where a hidden platform was placed (right or left to avoid side biases). Upon reaching the platform, which completes the task, mice are rewarded by being allowed to return to their cages. Every day consisted of three trials. During normal phase swimming (i.e. days 2–7), the mice from all groups learned the task and made more correct choices over the course of the test (Fig. 3A). We observed no difference among genotypes performing the task during the 7-day trial. Thus, the BACHD and DTg groups learned to find the platform similar to their control littermates (Fig. 3B). The time to reach the platform (Fig. 3D), the swim velocity and the distance taken to reach the platform were not different among groups.

To assess the ability of BACHD mice to change strategy, we incorporated a reversal phase into the swimming T-maze test by switching the platform to the opposite arm of the maze. Mice that were trained to swim directly to the right or left arm would now have to change their strategy to find the shortest path to the platform. WT, Cryab Tg and DTg mice swam down the arm in which they were trained initially and, after discovering that the platform was no longer present, immediately swam down the unvisited opposite arm of the maze and found the platform. Similar to the WT mice, all of the BACHD mice entered the arm of the T-maze they were initially trained to. However, after discovering that the platform was not present in the opposite arm of the maze, the majority of the BACHD mice swam back to the start of the T-maze where they had already been. We measured this abnormality by quantifying the number of arms of the maze entered en route to the platform. This pattern of response resulted in the BACHD mice having more arm entries than WT, Cryab Tg and DTg mice, as it was apparently more difficult for the BACHD group to attain the 50% correct arm entries in the reversal arm over the course of the test (Fig. 3C). These results are consistent with findings observed in HD patients: during a re-learning process, HD patients tend to perseverate and have more difficulties in strategy shifting, than healthy subjects (45–51). The difference between the number of correct entries of the BACHD group was significantly lower (below 50%) than in the DTg group from Day 3 to Day 5 in the reversal test. In addition, DTg mice took significantly less time to relocate the hidden platform (Fig. 3E) than BACHD mice. DTg mice were not different from the WT and Cryab Tg groups.

αBc overexpression modulates levels of mhtt and inclusion body formation BACHD mice

To determine if the improved motor and cognitive behavioral phenotypes in DTg mice correlated with neuropathological

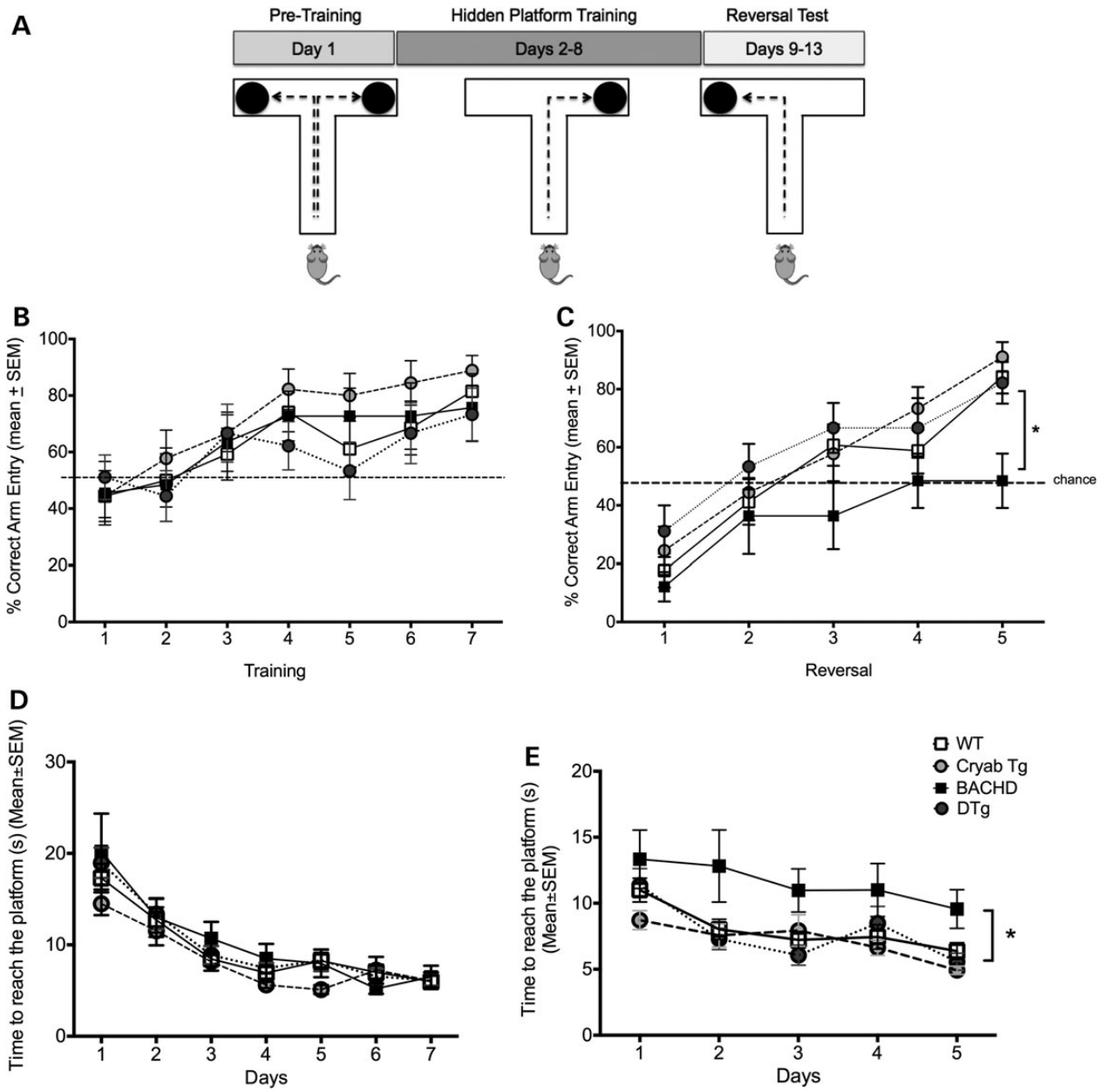

Figure 3. αBc overexpression improves BACHD strategy shifting in the water-T maze test. (**A**) Water-T maze test diagram. BACHD mice were tested in the swimming T-maze with reversal. At 13 months of age, group sizes were as follows: WT ($n = 18$), Cryab Tg ($n = 17$), BACHD ($n = 10$), DTg ($n = 15$). Symptomatic BACHD show cognitive deficits in strategy shifting, and αBc overexpression rescues this impairment. (**B**) During the normal phase of the test, the four distinct groups learned to swim to the platform, and no differences were observed in the percentage of correct arm entries, having the four groups reaching ≥80% of correct entries, and (**D**) in the time to reach the platform. (**C**) During the reversal phase, when the location of the platform was switched, BACHD mice showed a significant lower number of correct entries in the reversal arm and (**E**) required significantly more time to find the platform than the other groups from Day 3 to Day 5. Speed (cm/s) and distance (cm) to locate the platform in either training and reversal phases were not different among the four genotypes during this test performance. A two-way ANOVA was performed, with multiple comparisons tests, corrected by Tukey test. *$P < 0.05$.

changes, we examined disease features, such as inclusion body (IB) formation and neuronal cell loss. IB formation with mhtt is a hallmark of HD pathology. Aged BACHD mice develop IBs that are similar to those in the human disease and can be visualized histologically with specific htt antibodies. We examined serial sections from cortex and caudate–putamen/striatum of 13-month-old mice of this cohort and observed differences in the density or size of inclusion bodies. Staining with the polyclonal antibody S830, which selectively recognizes expanded mhtt (34,52), revealed prominent IBs in both the cortex and striatum of BACHD and DTG but not WT and Cryab Tg mice, as expected (Fig. 4C and D). Although there is a trend for a decrease of IB numbers in DTG when compared with BACHD, this difference did not reach statistical significance. However, there were significantly fewer larger inclusions (>1 μm) in DTg mice than in BACHD mice (Fig. 4D), indicating an overall reduction in size of inclusions.

The difference in IBs mediated by αBc suggested that other features of mhtt proteostasis might also be altered. Since expression level of mhtt is a strong predictor of neurodegeneration in polyQ transfected rodent primary neurons (53,54) and correlated

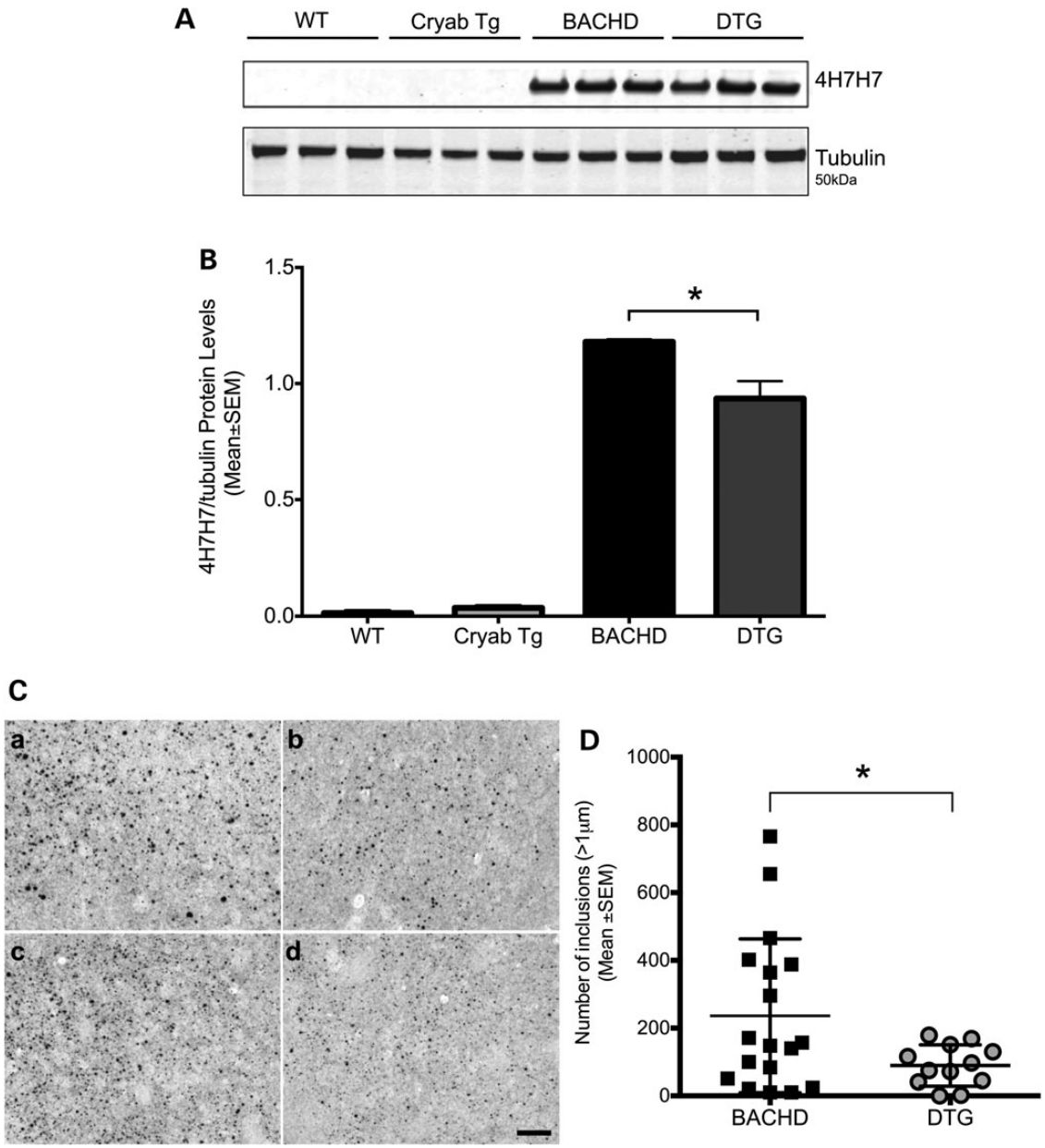

Figure 4. αBc overexpression decreases soluble levels of mhtt and reduces the size of S830 inclusion bodies in BACHD mice. (**A**) Representative western blot of WT, Cryab Tg, DTg and BACHD ($n = 4$) cortical lysates with 4H7H7 and anti-β-tubulin as a loading control and (**B**) subsequent quantification of signal intensity. Values are based on the mean of three independent 4H7H7 blots of four mice per group compared across different blots. All value were first normalized for input using the anti-β-tubulin controls. (**C**) Immunohistochemistry with polyoclonal S830 revealed prominent immunoreactive inclusion bodies in BACHD and DTg mice cortex and striatum but not in the WT and Cryab Tg littermate controls (data not shown). S830 immunohistochemistry in (a, c) BACHD and (b, d) DTg representative mouse brains with average levels of aggregate counts and density for the two groups: (a, b) M1/M2 cortex layer III and (c, d) striatum/medial caudate/putamen, using Renyi/Entropy threshold and >1 µm diameter. The scale bar represents 100 µm, and the field size is 205 µm × 150 µm. (**D**) The number of mhtt nuclear inclusions >1 µm were significantly reduced in the DTg when compared with BACHD mice. Values are means ± SD; BACHD ($n = 9$) and DTg ($N = 6$), $^*P < 0.05$ by Student's unpaired t-test.

with deficits in HD animal models (44), we compared the steady-state levels of soluble mhtt in cortical lysates.

Using the mouse monoclonal antibody 4H7H7, which preferentially recognizes pathogenic polyQ stretches (55), we found that DTg mice have a modest but reproducible and statistically significant reduction in soluble mhtt protein, compared with levels in BACHD mice (Fig. 4A and B). In summary, these results suggest that αBc is involved in modulating mhtt protein levels and mhtt IB size, two prominent hallmarks of HD pathogenesis.

αBc overexpression prevents cortical and striatal neurodegeneration caused by the expression of mhtt in BACHD mice

Pathological examination of brains of HD patients reveals profound atrophy and cell death of medium spiny neurons (MSNs) of the striatum, with cortical loss also a feature as the disease progresses (4). BACHD mice present intranuclear inclusions and also show selective degeneration of the MSNs, in addition to significant atrophy of the forebrain without accompanying changes

in the cerebellum (34), similar to the pattern of degeneration in human HD (56,57).

Having found that αBc overexpression improves both motor and cognitive-like phenotypes in BACHD mice and may help reduce the levels of the mhtt protein, we next sought to determine if the overexpression of αBc influences other neuropathological features of disease, looking at the striatum and cortex atrophy and/or cell loss. In BACHD brains at late stage of disease (13 months of age), more than 95% of MSNs express dopamine and cyclic AMP-regulated protein (32 kDa, also known as DARPP-32) (58). We have used a sophisticated system for quantitative immunofluorescence and morphometry to measure the expression of striatal spiny neuron-specific protein, DARPP-32, in BACHD, DTg, Cryab Tg and WT mice (Fig. 5A and B). We found fewer DARPP-32+ cells in BACHD striatum than in the other genotypes. In the DTg mice, the number of DARPP-32+ cells was similar to those on WT and Cryab Tg mice (Fig. 5A and B).

Although HD is predominantly associated with degeneration of the striatum, it also involves cortical areas (30). To measure striatal and cortical neuronal cell loss, we stained brain sections with the NeuN antibody, which recognizes neuron-specific nuclear protein (Fig. 5C–F). We observed a significant decrease of

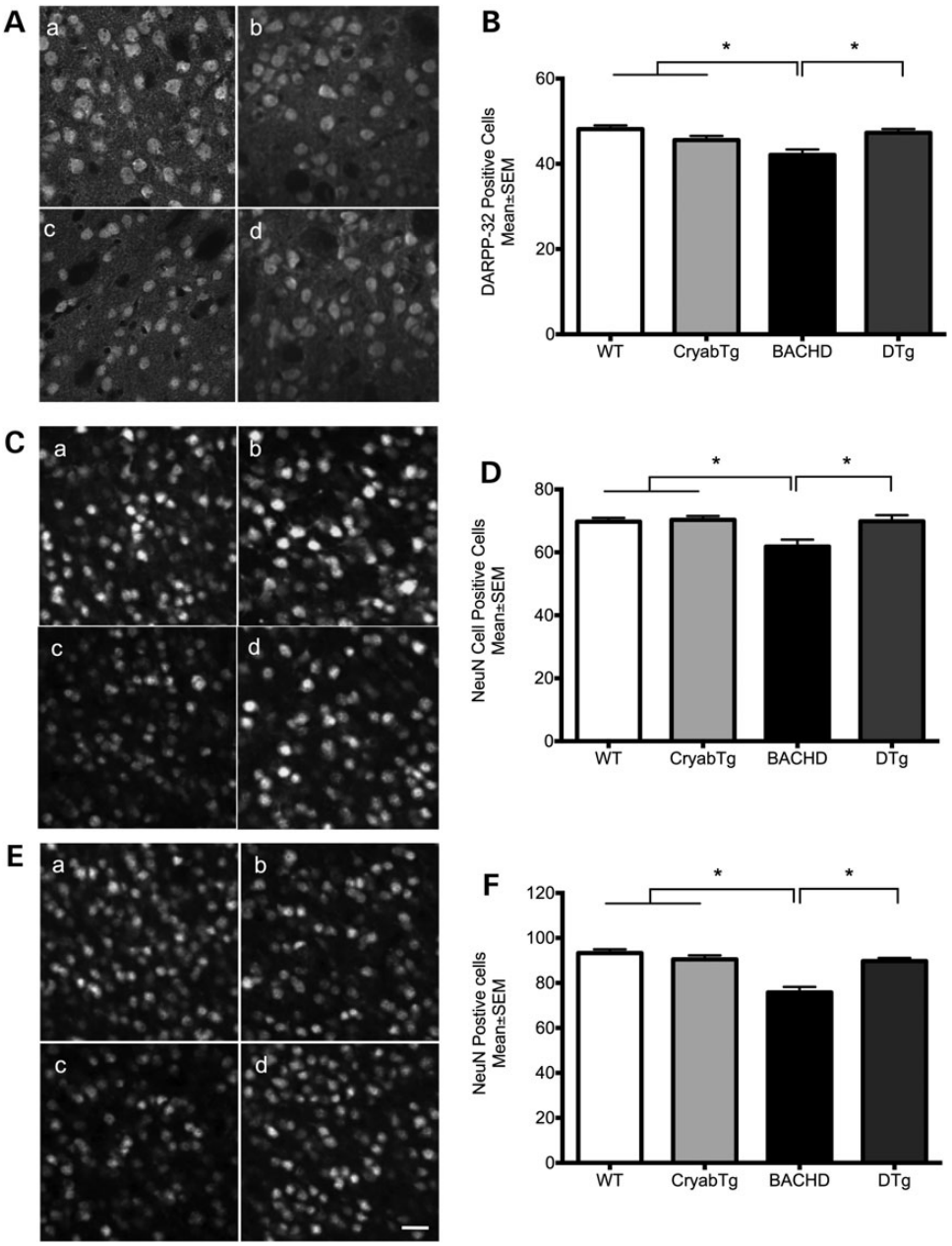

Figure 5. αBc overexpression rescues the neurodegeneration caused by expression of full-length mhtt at 13 months of age in BACHD. Measurement of striatal DARPP-32-positive cells and striatal cortical NeuN-positive cells in a: WT ($n = 5$), b: Cryab Tg ($n = 5$), c: BACHD ($n = 8$), d: DTg ($n = 7$). (**A**) Representative confocal micrographs of DARPP-32 immunostaining and (**B**) DARPP-32 positive cells quantification plots. (**C**, **E**) Representative confocal micrographs of NeuN immunostaining in the striatum/medial caudate/putamen (**C**) and M1/M2 cortex (**E**), followed by NeuN-positive cells quantification plots (**D**, **F**). Each field is 600 × 600 µm, and the scale bar represents 20 µm. Values represent means ± SEM. *$P < 0.05$, one-way ANOVA with multiple Tukey multiple comparisons correction.

both striatal (Fig. 5C and D) and cortical (Fig. 5E and F) NeuN+ counts when compared with WT mice, Cryab Tg and DTg mice. Taken together, our results indicate that astrocytic expression of αBc is associated with a significant reduction in striatal and cortical neuropathology in the BACHD model. Since astrocytic overexpression of αBc significantly mitigates pathology in neurons, it further suggests that αBc overexpression may be acting in a non-cell-autonomous manner.

Discussion

No therapeutics directly and effectively target and remediate the protein-misfolding events and selective neuronal vulnerability associated with many devastating neurodegenerative disorders (59). Therefore, approaches that target molecular chaperones may be beneficial in protein conformational diseases.

In this study, we report for the first time the effect of the sHsp αBc in a full-length mhtt model, the BACHD mouse. Expression of αBc in astrocytes improved the motor (RotaRod and Balance Beam) and cognitive performance (Water-T-maze) of the BACHD mice, as well as neuropathological features associated with HD. Overall, our data indicate that modulating the levels of αBc protect against the progression of HD.

We hypothesize that αBc has an important modulatory role during HD because the ability to effectively initiate the heat shock response (HSR), and other homeostatic cellular pathways (e.g. apoptosis, oxidative stress) in which αBc functions, are compromised during HD disease progression (60). We should also take into account, as a chaperone with multi-functional capabilities, αBc may alleviate stress by promoting ubiquitin/proteasomal degradation of corrupt proteins (61,62), preventing apoptosis (63–66) or by stabilizing intermediate filaments and the cytoskeleton integrity (67,68).

The most obvious candidate mechanism for chaperone-mediated rescue of HD neurotoxicity is inhibiting or reversing htt aggregate (fibrils/polymers) formation. Although mhtt is expressed in glial cells, the neuronal population contains most of mhtt aggregates (4,69). Our results indicate that αBc modulates mhtt levels and the features of IBs in a typical chaperone manner. Interestingly, however, the effect of this chaperone is via overexpressing αBc in astrocytes. Overexpression of chaperones may reduce large IBs by preventing oligomer formation, and oligomeric precursors may be the most toxic species (6,70,71). As with most Hsps, sHps can also be important for protein stability and protein turnover. Evidence suggests that affinity of αBc for its chaperone substrates is modulated by its chaperone oligomerization status and the functional structure of αBc is a dimer, which results from interactions of β-strands in the α-crystallin domain (72,73). Since the binding capacity can reach one substrate protein per sHsp subunit, big chaperone oligomer structures (via sHsp oligomerized complexes) are major contributors to the chaperoning capacity of the cell. It remains unclear how the decision to refold or degrade a misfolded protein is made. Some small sHsps (αBc and Hsp27) interact directly or indirectly with the proteasome and form part of ubiquitin ligase complexes (αBc and HspB10) that are involved in the proteasomal degradation of certain proteins in a quite selective manner under stress conditions (74). Thus, αBc could regulate mhtt protein levels by stabilizing mhtt in IBs or by promoting misfolded mhtt refolding with the cooperative help of other chaperone complexes, namely the Hsp70/Hsp40 machinery, as well as targeting it for proteosomal degradation.

But how could astrocytic αBc mediate this effect on neuronal aggregation and mhtt levels? αBc is secreted in exosomes under a variety of stress-related conditions (75). One possible mechanism of modulating neuronal IBs could be through αBc-mediated extracellular signaling from astrocytes to neurons. There is emerging evidence that astrocyte-derived exosomes carry neuroprotective cargo and could contribute to neuronal survival (76). Exosomes may execute their functions by distinct modes of action: (1) internalization by target cells and cargo retrieval, (2) binding to the cell surface and triggering second messenger pathways and (3) release of components into the extracellular matrix. However, their interaction as well as their protein content with target cells is not well understood at a mechanistic level (76). A study using retinal pigment epithelial (RPE) cells (77) showed that an increased uptake of exogenous αBc and protection from oxidative stress and apoptosis by inhibition of caspase 3 and PARP activation were observed in stressed RPE cultures. In this manner, we speculate that exosomes containing αBc could protect both glia and neuronal population in BACHD from mhtt-derived toxicity, as activation of caspase 3 and oxidative stress. Future studies will be necessary to test this hypothesis.

In our BACHD model, we additionally observed that astrocytic αBc overexpression resulted in protection of MSNs in the striatum, as well as cortical neurons. This rescue effect of astrocytic αBc on neurons further suggests that αBc confers neuroprotection in a non-cell-autonomous manner. The vast range of astrocytic functions, such as maintaining homeostasis at the synapse, regulating neuronal signaling, protecting neurons from oxidative damage and glutamate uptake, may have wide-ranging implications for the pathogenesis of protein aggregation disorders (78,79). HD, PD, spinocerebellar ataxia and ALS all demonstrate non-cell-autonomous pathology in which glial expression of mutant proteins has a toxic effect on vulnerable neurons, suggesting this may be a common feature of neurodegenerative disorders (80). In addition, a marked decreased expression of both glutamate transporters, GLAST and GLT-1, and of glutamate uptake, in a HD mouse model, were associated with neuronal dysfunction as observed by a reduction of the DARPP-32 and NR2B expression (31). Also, viral delivery of potassium channels (Kir4.) to striatal astrocytes restored Kir4.1 function, normalized extracellular K(+), ameliorated aspects of MSN dysfunction, prolonged survival and attenuated some motor phenotypes in R6/2 mice (32). These studies together may suggest astrocytes and ion channels and astrocytic-mediated transport as therapeutic targets. Interestingly, αBc overexpression was shown to maintain astrocyte functions such as glutamate uptake in AxD mouse model (26); however, we could not observe the same result in the BACHD mice. Further studies will be necessary to test αBc overexpression in astrocytic-mediated ion transport and ion channels expression in HD.

Co-culture of neurons with astrocytes from WT or BACHD mice identified mutant astrocytes as a source of adverse non-cell-autonomous effects on neuron energy metabolism possibly by increasing oxidative stress (81). Therefore, BACHD astrocytes may fail to provide adequate metabolic support to neurons. As αBc overexpression in astrocytes is sufficient to protect BACHD neurons in our study, it is possible that αBc is helping to restore metabolic support in astrocytes (e.g. antioxidant protection and glucose uptake) in DTg mice, protecting the neighboring neuronal population from mhtt-derived toxicity. Also, the chaperoning ability of αBc could be functioning to restore dysfunctional proteostasis in a general manner in astrocytes, leading to improvement in astrocyte health and astrocyte-to-neuron signaling. Overall, our studies indicate that astrocyte-mediated neuronal protection could be an important component of a therapeutic strategy for HD and other degenerative disorders with glial involvement.

In summary, our findings show that elevation of αBc in astrocytes may protect vulnerable neurons from mhtt toxicity, which could lead to improvements in motor behavior and cognition, as well as protecting against neuropathological deficits during BACHD disease progression. Our data are consistent with the possibility that metabolic deficiency in HD astrocytes plays a significant role in disease progression. Restoration of this deficiency by chaperones, such as αBc, may represent a mechanism of neuroprotection. Although the precise mechanism by which αBc overexpression alleviates neurodegeneration in BACHD is not fully understood, future studies will help to unravel the function of αBc in complex interactions with mHtt and potential other stressor targets in HD.

Materials and Methods

Animals and breeding strategy

Experiments involving mice were approved by the Institutional Animal Care and Use Committee of the University of California, San Francisco. Mice were housed, bred and maintained in compliance with National Institutes of Health guidelines. BACHD (BACHD^{tg}) mice (34) were obtained from William Yang (University of California, Los Angeles). Cryab Tg (Cryab^{tg}) mice with WT hamster Cryab gene under the control of the human GFAP promoter (26) were obtained from Albee Messing (University of Wisconsin, Madison). Both lines were maintained by breeding to WT FVB/NJ animals from the Jackson Laboratory (Bar Harbor, ME). To test if overexpression of αBc improved HD progression, we crossed the Cryab Tg mice to BACHD mice. Progeny from this breeding included Cryab^{Tg}, BACHD, Cryab^{tg};BACHD (double transgenic, DTg) and littermate controls, WT mice and were used for behavioral studies and HD-associated neuropathological studies.

Genotyping

Mouse-tail DNA was analyzed by PCR to determine the genotypes. The BACHD transgene was identified as described (34). The Cryab transgene was identified as described (80).

Behavioral assays

For all behavior experiments, experimenters were blinded to genotype. Experimental readouts were analyzed at 3, 7, 10 and 13 months for rotarod and balance beam to evaluate HD phenotype progression. All cages contained at least one mouse from each genotype, and mice were given environmental enrichment. Mice were subject to a 12-h light/dark cycle. Behavioral analysis of WT, Cryab Tg, BACHD and DTg mice was done blind to genotype.

Before starting the behavioral analyses at the first time point (3 months), two mice from our cohort presented tumors in their legs (one was WT and the other BACHD). In our water-T-maze study (at 13 months), one mouse (from the double transgenic—DTg group) was removed from testing because he was an aggressive male that bit the tester during the pre-training phase. This mouse's aggressive behavior resulted in the need to house this mouse singly and to be excluded from the last behavioral assay. In both cases, these mice were excluded, but the exclusion was not based on behavioral performance and so did not introduce an obvious bias into the measurements.

Rotarod

An accelerating rotarod (Med Associates ENV-577M) was used to analyze motor coordination and balance. Baseline behavior was performed at 3 months, and mice were placed into balanced cohorts based on sex, and genotype. Mice were trained three times at a constant speed of 16 rpm for maximum of 300 s. During testing, mice were subjected to beam acceleration of 4–40 rpm for a maximum of 300 s, three times per session (1 day) for a total of three sessions/days (39). Performance was quantified by measuring the latency to fall off of the rotarod apparatus.

Balance beam

The balance beam was also used to assess motor coordination and balance. This test consisted of three sessions with three trials in each session: one session of training, one session of testing on large diameter beam and one session of testing on medium diameter beam. Motor performance was assessed by measuring the time it takes for the mouse to traverse the beam, the number of hind paw slips and the number of falls during this process (37).

Water T-maze

Normal phase swimming T-maze test

The full-length mHtt model—YAC128 mice—show multiple cognitive deficits in swimming T-maze test (44). We decided to test cognitive deficits in BACHD mice at 13 months.

Mice were tested to assess spatial learning and memory. They were placed in the base of a water-filled T-maze and trained to swim to an escape platform located in the right or left arm of the maze (mice were divided in two groups and trained to reach the platform to the right or to the left side to be unbiased in the test). Mice must learn to turn to the correct arm to reach the platform directly.

During this test, mice received three trials per day for 7 days. To successfully complete this task, mice must remember either the location of or the path to the escape platform. Because FVB/N mice have severe retinal degeneration at the age tested (81), learning to swim to the correct arm of the maze likely relies on internal rather than external cues.

Reversal phase swimming T-maze test

After 1 day of rest, we included a reversal phase to the swimming T-maze test to assess the ability of the mice to replace a previously learned strategy. For this test, the platform was switched to the opposite arm (used in the first phase) of the T-maze. Mice received three trials per day for 5 days.

For the two phases of the T-maze test, the time to reach the platform, the swim velocity and the distance taken to reach the platform were recorded. Swimming through the incorrect arm was arbitrarily given a score of 0, whereas swimming into the correct arm where the platform was located was given a score of 1.

Protein extraction

Mice were anesthetized with Avertin (tribromoethanol, 250 mg per kg) and perfused transcardially with 0.9% saline. Brains were removed, microdissected in ice-cold PBS and homogenized in ice-cold standard RIPA buffer (150 mM NaCl, 1% NP-40, 0.1% sodium dodecyl sulfate, 0.5% sodium deoxycholate, 50 mM Tris, pH 7.4) supplemented with complete protease inhibitors (Roche Applied Science) and spun at 14 000 × *g* for 20 min at 4°C.

Western blotting

Proteins (10–20 μg/well) were separated on a 4–12% NuPAGE Bis-Tris gel (Life Technologies) and transferred onto nitrocellulose membranes, which were incubated for 1 h in 5% bovine serum

albumin (Sigma-Aldrich) diluted in Tris-buffered saline containing 0.05% Tween (BSA-TBST). Immunoblots were probed and incubated overnight at 4°C in rabbit anti-αBc (1:1000, Stressgen), 4H7H7 (1:5000), 1C2, (Millipore, MAB1574, 1:3000), anti-Htt 2166 (Millipore, mAb2166, 1:3000) or anti-B-tubulin (Abcam, ab6046, 1:20000) antibodies diluted in BSA-TBST. Appropriate IRDye secondary antibodies (LI-COR Biosci) were used at a 1:20 000 dilution. Images were captured with the Odyssey CLx (LI-COR Biosci).

Neuropathology

Mice were anesthetized with avertin (tribromoethanol, 250 mg/kg) and perfused with saline. Hemi-brains were then drop fixed in 4% paraformaldehyde for 48 h. For mhtt inclusions, multiple perfusion-fixed brains were embedded in gelatin blocks, post-fixed and freeze-cut into coronal 35 μm sections in 24 sequential series (NeuroScience Associates Inc., Knoxville, TN). These were stored at −20°C in cryoprotectant as individual series of sections and stained for mhtt-derived aggregates with an affinity purified preparation of the sheep anti-htt antibody S830 (30 ng/mL) under uniform free-floating conditions modified from previous descriptions (82). Binding was visualized using ultra-sensitive HRP-based Ni++/DAB immunohistochemistry. Images (590 μ × 470 μ) were collected with a Nikon DS-RI1 Digital Sight camera on a Nikon Eclipse Ni microscope under control of NIS-Elements V4.30. Extended depth-of-field images were converted to gray scale and numbers and size of immunoreactive inclusion bodies determined using Fiji-ImageJ.

For striatal and cortical counts: Fixed brains were sectioned into 40 μm sections with a Leica Vibratome in 24 sequential series. Free-floating sections were incubated in either 10% goat or donkey serum in 0.1% Triton X-100 for 1 h before incubation with primary antibodies at 4°C for 24 h. Sections were then immunostained with anti-DARPP32 (1:1000, Cell Signaling) and NeuN (1:1000, Chemicon). The specific areas analyzed were striatum/medial caudate/putamen and M1/M2 cortex. For all neuropathological analysis, at least three sections were analyzed per mouse and for each section and each area (cortex or striatum), we obtained six to seven fields of view/micrographs and cell counts were averaged per area/per mice. For comparison across genotypes, we selected sections from the same sequential series. Confocal micrographs for DARPP-32- and NeuN-positive cells were analyzed with original proprietary programs that were written in MATLAB.

The following steps used on a Matlab Script were used for all images from the different groups of mice and analyzed simultaneously.

1. The script first reads the input image and filters it using an adaptive thresholding method based on the paper 'Adaptive Thresholding for the DigitalDesk' by Pierre Wellner (83). We used median filtering and relative thresholds instead of absolute as they gave more accurate results.
2. After thresholding, we end up with a binary image where the objects of interest are labeled with 1's. This image also has some noise in the form of small white objects that need to be removed. Hence, we use morphology to remove all objects that are smaller than 200 pixels in area. This helps cleanup the thresholded image, and we are left with the cells of interest (that will be examined/reviewed to counteract possible shrunken and smaller cells to avoid therefore a different cell count in one of the genotypes compared with the other; this revision is done blindly for each genotype). The images below illustrate the application of this algorithm to image data, and demonstrate that the program is capable of accurately identifying and counting cells as objects, despite a fairly wide variation in cell size and morphology.
3. After morphological cleanup, we still need to process these images further because there may be touching cells that need to be separated. This is done using a recursive watershed method to split merged objects, as described in (84) for the iterative watershed method.
4. At this point, we now have separate objects in each image that we count for each image. (see example in the Supplementary Material, Fig. S3).

The program applies a constant threshold for pixel intensity to quantify cell diameter among four genotypes in an unbiased manner. Results from the analysis program were reviewed and minimally hand curated to avoid artifacts (false-negative cells) and to make sure that if neurons did shrink in size, they did not fall below a certain area to be counted. For all studies, the experimenter was blind to the genotype of the mice.

Statistical analyses

All data are expressed as the mean ± SEM. Variances between two groups were compared by *F*-test and differences between two groups by unpaired Student's *t*-test (two-tailed, unless indicated otherwise in the figure legends). Differences among multiple groups were assessed by one-way or two-way ANOVA, followed by Tukey multiple comparisons post-hoc tests, as specified in the figure legends. Correlations were assessed by linear regression and Spearman's correlation. Null hypotheses were rejected at $P < 0.05$. All statistical analysis was performed using Prism (Graphpad, GraphPad Prism v6.0; GraphPad Software La Jolla, CA).

To address concerns related with winner's curse on our data, we presented a very common summary statistic, Cohen's *d*, whose single value can be plugged directly into standard statistical software (such as R, SAS, SPSS, STATA) or online sample size calculators (http://www.danielsoper.com/statcalc3/calc.aspx?id=47) to calculate the required sample size. If readers want to address issues of potential upward bias of the effect size, they could scale the estimate of the Cohen's *d* by say 30% and then use this smaller effect size to calculate the necessary sample size (Supplementary Material, Tables S1–S5).

Supplementary Material

Supplementary Material is available at *HMG* online.

Acknowledgements

We thank Dr Albee Messing for generously providing Cryab transgenic mice and Dr William Yang for generously providing BACHD transgenic mice. We are grateful to Dr Rebecca Aron for stimulating scientific discussions, experimental advice and enormous help in editing the manuscript. We also thank Siddharth Samsi for very helpful advice and assistance with confocal imaging analysis and the members of the Finkbeiner lab for helpful discussions; Dr Gillian Bates for generously providing S830 antiserum; Iris Lo, Michael Gill and the Gladstone Institutes Behavioral Core for training and assistance with behavioral assays (supported by NIH grant P30NS065780); Cliff Anderson-Bergman, Grisell Diaz Ramirez and Michael Gill for biostatistics discussions; Dr Meredith Calvert for immunohistochemistry and histology advice; Kurt Thorn and DeLaine Larsen at the UCSF Nikon Imaging Center for training and assistance with confocal imaging; Gary

Howard for editorial assistance and Kelley Nelson for administrative support.

Conflict of Interest statement: The authors declare that no conflict of interest exists.

Funding

A.O.O. was supported by the doctoral fellowship SFRH/BD/65942/2009 from Fundação para Ciência e Tecnologia. Work in the lab of S.F. was supported by National Institutes of Neurological Disorders and Stroke grants 3R01 NS039074 and 2R01 NS045091, the Taube/Koret Center for Neurodegenerative Disease and the Hellman Family Foundation Alzheimer's Disease Research Program. T.F.O is supported by the DFG Center for Nanoscale Microscopy and Molecular Physiology of the Brain. The Gladstone Institutes received support from a National Center for Research Resources Grant RR18928.

References

1. Landles, C. and Bates, G.P. (2004) Huntingtin and the molecular pathogenesis of Huntington's disease. Fourth in molecular medicine review series. *EMBO Rep.*, **5**, 958–963.
2. Finkbeiner, S. (2011) Huntington's disease. *Cold Spring Harb. Perspect. Biol.*, **3**, 74–86.
3. Gil, J.M. and Rego, A.C. (2008) Mechanisms of neurodegeneration in Huntington's disease. *Eur. J. Neurosci.*, **27**, 2803–2820.
4. Vonsattel, J.P. (1998) Huntington's disease. *J. Neuropathol. Exp. Neurol.*, **57**, 369–384.
5. Lindquist, S. (1986) The heat-shock response. *Ann. Rev. Biochem.*, **55**, 1151–1191.
6. Muchowski, P.J. and Wacker, J.L. (2005) Modulation of neurodegeneration by molecular chaperones. *Nat. Rev. Neurosci.*, **6**, 11–22.
7. Wyttenbach, A. (2004) Role of heat shock proteins during polyglutamine neurodegeneration. *J. Mol. Neurosci.*, **23**, 69–95.
8. Wyttenbach, A., Carmichael, J., Swartz, J., Furlong, R.A., Narain, Y., Rankin, J. and Rubinsztein, D.C. (2000) Effects of heat shock, heat shock protein 40 (HDJ-2), and proteasome inhibition on protein aggregation in cellular models of Huntington's disease. *Proc. Natl. Acad. Sci. USA*, **97**, 2898–2903.
9. Vos, M.J., Zijlstra, M.P., Kanon, B., van Waarde-Verhagen, M.A., Brunt, E.R.P., Oosterveld-Hut, H.M.J., Carra, S., Sibon, O.C.M. and Kampinga, H.H. (2010) HSPB7 is the most potent polyQ aggregation suppressor within the HSPB family of molecular chaperones. *Hum. Mol. Genet.*, **19**, 4677–4693.
10. Warrick, J.M., Chan, H.Y., Gray-Board, G.L., Chai, Y., Paulson, H.L. and Bonini, N.M. (1999) Suppression of polyglutamine-mediated neurodegeneration in Drosophila by the molecular chaperone HSP70. *Nat. Genet.*, **23**, 425–428.
11. Garrido, C., Paul, C., Seigneuric, R. and Kampinga, H.H. (2012) The small heat shock proteins family: the long forgotten chaperones. *Int. J. Biochem. Cell Biol.*, **44**, 1588–1592.
12. Hayes, D., Napoli, V., Mazurkie, A., Stafford, W.F. and Graceffa, P. (2009) Phosphorylation dependence of Hsp27 multimeric size and molecular chaperone function. *J. Biol. Chem.*, **284**, 18801–18807.
13. Robertson, A.L., Headey, S.J., Saunders, H.M., Ecroyd, H., Scanlon, M.J., Carver, J.A. and Bottomley, S.P. (2010) Small heat-shock proteins interact with a flanking domain to suppress polyglutamine aggregation. *Proc. Natl. Acad. Sci. USA*, **107**, 10424–10429.
14. Carver, J.A., Rekas, A., Thorn, D.C. and Wilson, M.R. (2003) Small heat-shock proteins and clusterin: intra- and extracellular molecular chaperones with a common mechanism of action and function? *IUBMB Life*, **55**, 661–668.
15. Ecroyd, H. and Carver, J.A. (2009) Crystallin proteins and amyloid fibrils. *Cell. Mol. Life Sci.*, **66**, 62–81.
16. Westerheide, S.D. and Morimoto, R.I. (2005) Heat shock response modulators as therapeutic tools for diseases of protein conformation. *J. Biol. Chem.*, **280**, 33097–33100.
17. Muchowski, P.J., Schaffar, G., Sittler, A., Wanker, E.E., Hayer-Hartl, M.K. and Hartl, F.U. (2000) Hsp70 and hsp40 chaperones can inhibit self-assembly of polyglutamine proteins into amyloid-like fibrils. *Proc. Natl. Acad. Sci. USA*, **97**, 7841–7846.
18. Satyal, S.H., Schmidt, E., Kitagawa, K., Sondheimer, N., Lindquist, S., Kramer, J.M. and Morimoto, R.I. (2000) Polyglutamine aggregates alter protein folding homeostasis in *Caenorhabditis elegans*. *Proc. Natl. Acad. Sci. USA*, **97**, 5750–5755.
19. Jana, N.R., Tanaka, M., Wang, G.H. and Nukina, N. (2000) Polyglutamine length-dependent interaction of Hsp40 and Hsp70 family chaperones with truncated N-terminal huntingtin: their role in suppression of aggregation and cellular toxicity. *Hum. Mol. Genet.*, **9**, 2009–2018.
20. Hay, D.G., Sathasivam, K., Tobaben, S., Stahl, B., Marber, M., Mestril, R., Mahal, A., Smith, D.L., Woodman, B. and Bates, G.P. (2004) Progressive decrease in chaperone protein levels in a mouse model of Huntington's disease and induction of stress proteins as a therapeutic approach. *Hum. Mol. Genet.*, **13**, 1389–1405.
21. Horwitz, J. (2003) Alpha-crystallin. *Exp. Eye Res.*, **76**, 145–153.
22. Rekas, A., Adda, C.G., Andrew Aquilina, J., Barnham, K.J., Sunde, M., Galatis, D., Williamson, N.a., Masters, C.L., Anders, R.F., Robinson, C.V. *et al.* (2004) Interaction of the molecular chaperone alphaB-crystallin with alpha-synuclein: effects on amyloid fibril formation and chaperone activity. *J. Mol. Biol.*, **340**, 1167–1183.
23. Waudby, C.A., Knowles, T.P.J., Devlin, G.L., Skepper, J.N., Ecroyd, H., Carver, J.A., Welland, M.E., Christodoulou, J., Dobson, C.M. and Meehan, S. (2010) The interaction of αB-crystallin with mature α-synuclein amyloid fibrils inhibits their elongation. *Biophys. J.*, **98**, 843–851.
24. Hochberg, G.K.A., Ecroyd, H., Liu, C., Cox, D., Cascio, D., Sawaya, M.R., Collier, M.P., Stroud, J., Carver, J.A., Baldwin, A.J. *et al.* (2014) The structured core domain of αB-crystallin can prevent amyloid fibrillation and associated toxicity. *Proc. Natl. Acad. Sci. USA*, **111**, 1562–1570.
25. Wang, J., Xu, G., Li, H., Gonzales, V., Fromholt, D., Karch, C., Copeland, N.G., Jenkins, N.A. and Borchelt, D.R. (2005) Somatodendritic accumulation of misfolded SOD1-L126Z in motor neurons mediates degeneration: αB-crystallin modulates aggregation. *Hum. Mol. Genet.*, **14**, 2335–2347.
26. Hagemann, T.L., Boelens, W.C., Wawrousek, E.F. and Messing, A. (2009) Suppression of GFAP toxicity by alphaB-crystallin in mouse models of Alexander disease. *Hum. Mol. Genet.*, **18**, 1190–1199.
27. Muchowski, P.J., Ramsden, R., Nguyen, Q., Arnett, E.E., Greiling, T.M., Anderson, S.K. and Clark, J.I. (2008) Non-invasive measurement of protein aggregation by mutant huntingtin fragments or alpha-synuclein in the lens. *J. Biol. Chem.*, **283**, 6330–6336.
28. Tue, N.T., Shimaji, K., Tanaka, N. and Yamaguchi, M. (2012) Effect of alphab-crystallin on protein aggregation in drosophila. *J. Biomed. Biotechnol.*, **20**, 12–18.

29. Zabel, C. (2002) Alterations in the mouse and human proteome caused by Huntington's disease. *Mol. Cell. Proteomics*, **1**, 366–375.
30. Ehrlich, M.E. (2012) Huntington's disease and the striatal medium spiny neuron: cell-autonomous and non-cell-autonomous mechanisms of disease. *Neurotherapeutics*, **9**, 270–284.
31. Faideau, M., Kim, J., Cormier, K., Gilmore, R., Welch, M., Auregan, G., Dufour, N., Guillermier, M., Brouillet, E., Hantraye, P. *et al.* (2010) In vivo expression of polyglutamine-expanded huntingtin by mouse striatal astrocytes impairs glutamate transport: a correlation with Huntington's disease subjects. *Hum. Mol. Genet.*, **19**, 3053–3067.
32. Tong, X., Ao, Y., Faas, G.C., Nwaobi, S.E., Xu, J., Haustein, M.D., Anderson, M.A., Mody, I., Olsen, M.L., Sofroniew, M.V. *et al.* (2014) Astrocyte Kir4.1 ion channel deficits contribute to neuronal dysfunction in Huntington's disease model mice. *Nat. Neurosci.*, **17**, 694–703.
33. Boussicault, L., Hérard, A.-S., Calingasan, N., Petit, F., Malgorn, C., Merienne, N., Jan, C., Gaillard, M.-C., Lerchundi, R., Barros, L.F. *et al.* (2014) Impaired brain energy metabolism in the BACHD mouse model of Huntington's disease: critical role of astrocyte-neuron interactions. *J. Cereb. Blood Flow Metab.*, **10**, 22–34.
34. Gray, M., Shirasaki, D.I., Cepeda, C., André, V.M., Wilburn, B., Lu, X.-H., Tao, J., Yamazaki, I., Li, S.-H., Sun, Y.E. *et al.* (2008) Full-length human mutant huntingtin with a stable polyglutamine repeat can elicit progressive and selective neuropathogenesis in BACHD mice. *J. Neurosci.*, **28**, 6182–6195.
35. Slow, E.J., van Raamsdonk, J., Rogers, D., Coleman, S.H., Graham, R.K., Deng, Y., Oh, R., Bissada, N., Hossain, S.M., Yang, Y.Z. *et al.* (2003) Selective striatal neuronal loss in a YAC128 mouse model of Huntington disease. *Hum. Mol. Genet.*, **12**, 1555–1567.
36. Menalled, L., El-Khodor, B.F., Patry, M., Suárez-Fariñas, M., Orenstein, S.J., Zahasky, B., Leahy, C., Wheeler, V., Yang, X.W., MacDonald, M. *et al.* (2009) Systematic behavioral evaluation of Huntington's disease transgenic and knock-in mouse models. *Neurobiol. Dis.*, **35**, 319–336.
37. Bouchard, J., Truong, J., Bouchard, K., Dunkelberger, D., Desrayaud, S., Moussaoui, S., Tabrizi, S.J., Stella, N. and Muchowski, P.J. (2012) Cannabinoid receptor 2 signaling in peripheral immune cells modulates disease onset and severity in mouse models of Huntington's disease. *J. Neurosci.*, **32**, 18259–18268.
38. Kwan, W., Träger, U., Davalos, D., Chou, A., Bouchard, J., Andre, R., Miller, A., Weiss, A., Giorgini, F., Cheah, C. *et al.* (2012) Mutant huntingtin impairs immune cell migration in Huntington disease. *J. Clin. Invest.*, **122**, 57–68.
39. Larkin, P.B. and Muchowski, P.J. (2012) Genetic deficiency of complement component 3 does not alter disease progression in a mouse model of Huntington's disease. *J. Huntingtons. Dis.*, **29**, 997–1003.
40. Crook, Z.R. and Housman, D. (2011) Huntington's disease: can mice lead the way to treatment? *Neuron*, **69**, 423–435.
41. Abada, Y.-S.K., Nguyen, H.P., Ellenbroek, B. and Schreiber, R. (2013) Reversal learning and associative memory impairments in a BACHD rat model for Huntington disease. *PLoS One*, **8**, 716–733.
42. Paulsen, J.S., Langbehn, D.R., Stout, J.C., Aylward, E., Ross, C.A., Nance, M., Guttman, M., Johnson, S., MacDonald, M., Beglinger, L.J. *et al.* (2008) Detection of Huntington's disease decades before diagnosis: the Predict-HD study. *J. Neurol. Neurosurg. Psychiatry*, **79**, 874–880.
43. Paulsen, J.S., Ready, R.E., Hamilton, J.M., Mega, M.S. and Cummings, J.L. (2001) Neuropsychiatric aspects of Huntington's disease. *J Neurol. Neurosurg. Psychiatry*, **5**, 310–314.
44. Van Raamsdonk, J.M., Pearson, J., Slow, E.J., Hossain, S.M., Leavitt, B.R. and Hayden, M.R. (2005) Cognitive dysfunction precedes neuropathology and motor abnormalities in the YAC128 mouse model of Huntington's disease. *J. Neurosci.*, **25**, 4169–4180.
45. Hahn-Barma, V., Deweer, B., Durr, A., Dode, C., Feingold, J., Pillon, B., Agid, Y., Brice, A. and Dubois, B. (1998) Are cognitive changes the first symptoms of Huntington's disease? A study of gene carriers. *J. Neurol. Neurosurg. Psychiatry*, **64**, 172–177.
46. Lawrence, A.D., Sahakian, B.J., Hodges, J.R., Rosser, A.E., Lange, K.W. and Robbins, T.W. (1996) Executive and mnemonic functions in early Huntington's disease. *Brain*, **119**, 1633–1645.
47. Lawrence, A.D., Hodges, J.R., Rosser, A.E., Kershaw, A., Ffrench-Constant, C., Rubinsztein, D.C., Robbins, T.W. and Sahakian, B.J. (1998) Evidence for specific cognitive deficits in preclinical Huntington's disease. *Brain*, **121**, 1329–1341.
48. Lawrence, A.D., Sahakian, B.J. and Robbins, T.W. (1998) Cognitive functions and corticostriatal circuits: Insights from Huntington's disease. *Trends Cogn. Sci.*, **2**, 379–388.
49. Snowden, J.S., Craufurd, D., Thompson, J. and Neary, D. (2002) Psychomotor, executive, and memory function in preclinical Huntington's disease. *J. Clin. Exp. Neuropsychol.*, **24**, 133–145.
50. Thompson, J.C., Ph, D., Harris, J., Sc, B., Sollom, A.C., Stopford, C.L., Howard, E., Snowden, J.S., Craufurd, D. and Sc, M. (2012) Longitudinal evaluation of neuropsychiatric symptoms in Huntington's disease. *J. Neuropsychiatry Clin. Neurosci.*, **11**, 19–31.
51. Snowden, J.S., Gibbons, Z.C., Blackshaw, A., Doubleday, E., Thompson, J., Craufurd, D., Foster, J., Happé, F. and Neary, D. (2003) Social cognition in frontotemporal dementia and Huntington's disease. *Neuropsychologia*, **41**, 688–701.
52. Pouladi, M.A., Stanek, L.M., Xie, Y., Franciosi, S., Southwell, A.L., Deng, Y., Butland, S., Zhang, W., Cheng, S.H., Shihabuddin, L.S. *et al.* (2012) Marked differences in neurochemistry and aggregates despite similar behavioural and neuropathological features of Huntington disease in the full-length BACHD and YAC128 mice. *Hum. Mol. Genet.*, **21**, 2219–2232.
53. Miller, J., Arrasate, M., Brooks, E., Libeu, C.P., Legleiter, J., Hatters, D., Curtis, J., Cheung, K., Krishnan, P., Mitra, S. *et al.* (2012) Identifying polyglutamine protein species in situ that best predict neurodegeneration. *Nat. Chem. Biol.*, **8**, 308–318.
54. Miller, J., Arrasate, M., Shaby, B.A., Mitra, S., Masliah, E. and Finkbeiner, S. (2010) Quantitative relationships between huntingtin levels, polyglutamine length, inclusion body formation, and neuronal death provide novel insight into huntington's disease molecular pathogenesis. *J. Neurosci.*, **30**, 10541–10550.
55. Gu, X., Greiner, E.R., Mishra, R., Kodali, R., Osmand, A., Finkbeiner, S., Steffan, J.S., Thompson, L.M., Wetzel, R. and Yang, X.W. (2009) Serines 13 and 16 are critical determinants of full-length human mutant Huntingtin induced disease pathogenesis in HD mice. *Neuron*, **64**, 828–840.
56. Gourfinkel-An, I., Vila, M., Faucheux, B., Duyckaerts, C., Viallet, F., Hauw, J.J., Brice, A., Agid, Y. and Hirsch, E.C. (2002) Metabolic changes in the basal ganglia of patients with Huntington's disease: An in situ hybridization study of cytochrome oxidase subunit I mRNA. *J. Neurochem.*, **80**, 466–476.
57. Herndon, E.S., Hladik, C.L., Shang, P., Burns, D.K., Raisanen, J. and White, C.L. (2009) Neuroanatomic profile of

polyglutamine immunoreactivity in Huntington disease brains. *J. Neuropathol. Exp. Neurol.*, **68**, 250–261.
58. Ouimet, C.C., Langley-Gullion, K.C. and Greengard, P. (1998) Quantitative immunocytochemistry of DARPP-32-expressing neurons in the rat caudatoputamen. *Brain Res.*, **808**, 8–12.
59. Labbadia, J. and Morimoto, R.I. (2013) Huntington's disease: underlying molecular mechanisms and emerging concepts. *Trends Biochem. Sci.*, **38**, 378–385.
60. Arrigo, A.P., Simon, S., Gibert, B., Kretz-Remy, C., Nivon, M., Czekalla, A., Guillet, D., Moulin, M., Diaz-Latoud, C. and Vicart, P. (2007) Hsp27 (HspB1) and αB-crystallin (HspB5) as therapeutic targets. *FEBS Lett.*, **581**, 3665–3674.
61. den Engelsman, J., Keijsers, V., de Jong, W.W. and Boelens, W.C. (2003) The small heat-shock protein alpha B-crystallin promotes FBX4-dependent ubiquitination. *J. Biol. Chem.*, **278**, 4699–4704.
62. Lin, D.I., Barbash, O., Kumar, K.G.S., Weber, J.D., Harper, J.W., Klein-Szanto, A.J.P., Rustgi, A., Fuchs, S.Y. and Diehl, J.A. (2006) Phosphorylation-dependent ubiquitination of cyclin D1 by the SCFFBX4-αB crystallin complex. *Mol. Cell*, **24**, 355–366.
63. Kamradt, M.C., Lu, M., Werner, M.E., Kwan, T., Chen, F., Strohecker, A., Oshita, S., Wilkinson, J.C., Yu, C., Oliver, P.G. *et al.* (2005) The small heat shock protein alpha B-crystallin is a novel inhibitor of TRAIL-induced apoptosis that suppresses the activation of caspase-3. *J. Biol. Chem.*, **280**, 11059–11066.
64. Mao, Y.-W., Liu, J.-P., Xiang, H. and Li, D.W.-C. (2004) Human alphaA- and alphaB-crystallins bind to Bax and Bcl-X(S) to sequester their translocation during staurosporine-induced apoptosis. *Cell Death Differ.*, **11**, 512–526.
65. Kamradt, M.C., Chen, F., Sam, S. and Cryns, V.L. (2002) The small heat shock protein alphaB-crystallin negatively regulates apoptosis during myogenic differentiation by inhibiting caspase-3 activation. *J. Biol. Chem.*, **277**, 38731–38736.
66. Kamradt, M.C., Chen, F. and Cryns, V.L. (2001) The small heat shock protein alphaB-crystallin negatively regulates cytochrome c- and caspase-8-dependent activation of caspase-3 by inhibiting its autoproteolytic maturation. *J. Biol. Chem.*, **276**, 16059–16063.
67. Ghosh, J.G., Shenoy, A.K. and Clark, J.I. (2007) Interactions between important regulatory proteins and human alphaB crystallin. *Biochemistry*, **46**, 6308–6317.
68. Ghosh, J.G., Houck, S.A. and Clark, J.I. (2007) Interactive domains in the molecular chaperone human alphaB crystallin modulate microtubule assembly and disassembly. *PLoS One*, **2**, 24–31.
69. DiFiglia, M., Sapp, E., Chase, K.O., Davies, S.W., Bates, G.P., Vonsattel, J.P. and Aronin, N. (1997) Aggregation of huntingtin in neuronal intranuclear inclusions and dystrophic neurites in brain. *Science*, **277**, 1990–1993.
70. Arrasate, M., Mitra, S., Schweitzer, E.S., Segal, M.R. and Finkbeiner, S. (2004) Inclusion body formation reduces levels of mutant huntingtin and the risk of neuronal death. *Nature*, **431**, 805–810.
71. Takahashi, T. and Mihara, H. (2008) Peptide and protein mimetics inhibiting amyloid B-peptide aggregation. *Acc. Chem. Res.*, **41**, 1309–1318.
72. Quraishe, S., Asuni, A., Boelens, W.C., O'Connor, V. and Wyttenbach, A. (2008) Expression of the small heat shock protein family in the mouse CNS: differential anatomical and biochemical compartmentalization. *Neuroscience*, **153**, 483–491.
73. Quraishe, S. (2010) The sHsp expression signature in the brain and modulation in models of chronic neurodegeneration, Doctoral Thesis, University of Southampton, 1–305.
74. Lanneau, D., de Thonel, A., Maurel, S., Didelot, C. and Garrido, C. (2007) Apoptosis versus cell differentiation: role of heat shock proteins HSP90, HSP70 and HSP27. *Prion*, **1**, 53–60.
75. Kore, R.A. and Abraham, E.C. (2014) Inflammatory cytokines, interleukin-1 beta and tumor necrosis factor-alpha, upregulated in glioblastoma multiforme, raise the levels of CRYAB in exosomes secreted by U373 glioma cells. *Biochem. Biophys. Res. Commun.*, **453**, 326–331.
76. Frühbeis, C., Fröhlich, D. and Krämer-Albers, E.M. (2012) Emerging roles of exosomes in neuron-glia communication. *Front. Physiol.*, **3**, 1–7.
77. Sreekumar, P.G., Kannan, R., Kitamura, M., Spee, C., Barron, E., Ryan, S.J. and Hinton, D.R. (2010) αB crystallin is apically secreted within exosomes by polarized human retinal pigment epithelium and provides neuroprotection to adjacent cells. *PLoS One*, **5**, 1–13.
78. Chan, C.S. and Surmeier, D.J. (2014) Astrocytes go awry in Huntington's disease. *Nat. Neurosci.*, **17**, 641–642.
79. Zhang, Y. and Barres, B.A. (2010) Astrocyte heterogeneity: an underappreciated topic in neurobiology. *Curr. Opin. Neurobiol.*, **20**, 588–594.
80. Lobsiger, C.S. and Cleveland, D.W. (2007) Glial cells as intrinsic components of non-cell-autonomous neurodegenerative disease. *Nat. Neurosci.*, **10**, 1355–1360.
81. Taketo, M., Schroeder, A.C., Mobraaten, L.E., Gunning, K.B., Hanten, G., Fox, R.R., Roderick, T.H., Stewart, C.L., Lilly, F. and Hansen, C.T. (1991) FVB/N: an inbred mouse strain preferable for transgenic analyses. *Proc. Natl. Acad. Sci. USA*, **88**, 2065–2069.
82. Osmand, A.P., Berthelier, V. and Wetzel, R. (2006) Imaging polyglutamine deposits in brain tissue. *Methods Enzymol.*, **412**, 106–122.
83. Wellner, P.D. (1993) Adaptive thresholding for the DigitalDesk. *Eur. Tech. Rep.*, **110**, 1–17.
84. Samsi, S., Lozanski, G., Shana'ah, A., Krishanmurthy, A.K. and Gurcan, M.N. (2010) Detection of follicles from IHC-stained slides of follicular lymphoma using iterative watershed. *IEEE Trans. Biomed. Eng.*, **57**, 2609–2612.